

Ultra-compact radio sources and the isotropy and homogeneity of the Universe

J. C. Jackson^{1‡}

¹Division of Mathematics, School of Computing, Engineering and Information Sciences, Northumbria University, Newcastle NE1 8ST, UK

Abstract. A 2.29 GHz VLBI all-sky survey of ultra-compact radio sources has formed the basis of a number of cosmological investigations, which examine the relationship between angular-size and redshift. Here I use a sample of 468 such sources with $0.5 < z \leq 3.787$, to investigate the isotropy of the Universe. The sample is divided into hemispherical sub-samples, over an all-sky $5^\circ \times 5^\circ$ array, each of which is allowed to determine a value of Ω_m , assuming that we are living in a spatially flat homogeneous isotropic Λ CDM model. If we regard the latter as a null hypothesis, then it fails the test – the results show significant anisotropy, the smallest value of Ω_m being towards $(l, b) = (253.9, 24.1)^\circ$, the largest in the opposite direction. This is close to the CMB dipole axis, but in the obverse sense. This is interpreted as meaning that the Universe is not spatially homogeneous on the largest scales, and is better represented at late times by a spherically symmetric model with a density enhancement at its centre.

Keywords: cosmology: observations – cosmology: theory – large-scale structure of the Universe

1. Introduction

In the large the Universe around us exhibits a remarkable degree of spherical symmetry, the most stringent constraint on anisotropy being provided by observations of the Cosmic Microwave Background (CMB). The near isotropy of the latter was apparent at the time of its discovery (Penzias & Wilson 1965; Wilson & Penzias 1967). Early COBE results showed a dipole component of $\Delta T = 3.335$ mK (0.12 per cent), and a monopole temperature of 2.725 K (Kogut et al. 1993; Mather et al. 1999). After removing the dipole component the rms sky variation is $\Delta T = 45.3$ μ K (0.0017 per cent) (see for example Percival et al. 2002) over the multipole range $2 \leq l \leq 1500$. If we accept the Copernican principle then these observations mean that the Universe is homogeneous and isotropic; the corresponding Friedmann–Lemaître–Robertson–Walker (FLRW) framework has been the the basis of most studies in observational cosmology.

‡E-mail: john.jackson@northumbria.ac.uk

However, while the Copernican principle remains untested, inhomogeneous models should not be dismissed (Clarkson & Maartens 2010; Ellis 2011). I report here a test of isotropy based upon the angular-size/redshift relationship, using ultra-compact radio sources as standard measuring rods; these objects have angular diameters in the milliarcsecond (mas) range, and linear sizes of order several parsecs. In fact the test reveals significant anisotropy, a tentative interpretation of which is that the Universe is not spatially homogeneous on the largest scales, and is better represented at late times by a spherically symmetric model with a density enhancement at its centre. Antoniou & Perivolaropoulos (2010) have already looked at Union2 SnIa dataset in this context, which shows a similar anisotropy; my approach closely follows theirs. More recently, Longo (2012) has reported an anomaly in the angular distribution of quasar magnitudes, which is interpreted as evidence for a large-scale distant inhomogeneity.

2. Ultra-compact radio sources

The data to be used derive from an ancient VLBI survey of such sources at 2.29 GHz (Preston et al. 1985, hereafter referred to as P85). This survey employed a world-wide array of dishes, forming an interferometric system with an effective baseline of about 8×10^7 wavelengths; the survey gave total and correlated flux densities (fringe amplitudes) for 917 objects, S_t and S_c respectively. The ratio $\Gamma = S_c/S_t$ is a measure of fringe visibility, from which angular size can be estimated (Thompson, Moran & Swenson 1986; Gurvits 1994):

$$\theta = \frac{2\sqrt{-\ln \Gamma \ln 2}}{\pi B}, \quad (1)$$

where B is the interferometer baseline, in wavelengths.

The potential of P85 in this context was first noted by Gurvits (1994), who considered a sample comprising 258 objects with redshifts $z > 0.5$. Using the same data set, Jackson & Dodgson (1997) extended this work to the full Ω_m/Ω_Λ plane, finding best values $\Omega_m = 0.2$ and $\Omega_\Lambda = 0.8$, if the Universe is spatially flat, later refined to $\Omega_m = 0.24$, $\Omega_\Lambda = 0.76$ (Jackson 2004). The sample was updated with regard to redshift (Jackson & Jannetta 2006), to give 613 objects with $0.0035 \leq z \leq 3.787$, of which 468 have $z > 0.5$, which sub-set is used in this investigation. There are several reasons for ignoring sources with $z < 0.5$. As z falls below 0.5, the epoch of quasar formation comes to an end, and the nature of the population changes dramatically (see the cyan points in Fig. 1); there is a correlation between linear size and radio luminosity – the weaker sources are distinctly smaller, which would introduce an unacceptable selection bias. There is no evidence of such an effect when $z > 0.5$ (Jackson 2004); if it is there it is not pronounced. A residual bias should not appear to be anisotropic.

A model of these objects, which gives an account of their status as standard measuring rods, is discussed in Jackson (2004). The model is supported by VLBA images (Kovalev et al. 2005), which show a bright compact ‘core’ at the end of a one-sided jet; the ‘core’ is believed to be the base of a continuous jet, rather than the

nucleus of the object. Beamed emission from the compact core dominates the observed structure. The importance of D oppler beaming cannot be over-stated; the rest-frame linear size of mas source components is known to be an increasing function of wavelength (Marscher & Shaffer 1980; Pearson & Readhead 1981); at first sight this would mean that the effective linear size should actually be a decreasing function of z . However, as z increases a larger D oppler boost factor \mathcal{D} is required; it turns out that the ratio $\mathcal{D}/(1+z)$ is approximately fixed (Jackson 2004), so that the emitted frequency $\mathcal{D}\nu_r/(1+z)$ is also fixed, where ν_r is the fixed reception frequency. Note that this ratio is not necessarily unity, but the fact that it is fixed means that the interferometric angular sizes upon which this work is based are fit for purpose. This is another reason for ignoring sources with $z < 0.5$, which appear to be non-relativistic. Again a residual bias should not appear to be anisotropic.

A second point which needs clarification is resolution. With a baseline $B = 8 \times 10^7$, the Rayleigh resolution limit is about 2.6 mas. The mean angular size of the sources in question is 1.52 mas, somewhat below the Rayleigh limit. However, it is well-known that a simple interferometric technique can achieve a degree of super-resolution; the matter is discussed in detail in Kovalev et al. (2005). The limiting factor is signal-to-noise ratio SNR ; for a simple Gaussian source the limiting angular size is

$$\theta_{\text{lim}} = b \left[\frac{4 \ln 2}{\pi} \ln \left(\frac{SNR}{SNR - 1} \right) \right]^{1/2}, \quad (2)$$

where b is the half-power beam width, which I have taken to be half the fringe spacing, thus $b = (2B)^{-1}$. As to the appropriate SNR , two figures are mentioned in Preston et al. (1985). The first is described as a systematic error of about 10 per cent; a systematic percentage error should not affect measures of fringe visibility, but I note that the corresponding resolution is $\theta_{\text{lim}} = 0.20$ mas. The second figure is an absolute random error of 0.2 Jy in the correlated flux density, in which case the SNR would vary from source to source; the median SNR value for those sources used in this investigation is 17, giving $\theta_{\text{lim}} = 0.15$ mas. These figures are indicative, but do confirm that lack of adequate angular resolution is unlikely to be an issue here. (However, for a radically different point-of-view see Pashchenko & Vitrihchak 2011).

Fig. 1 is the angular-diameter/redshift diagram for the full sample of 468 sources discussed above. The continuous green line corresponds to the best-fitting spatially flat homogeneous isotropic Λ CDM model, characterized by two free parameters, the matter density Ω_m and the intrinsic linear size d . The best values are $\Omega_m = 0.29$ and $d = 7.76h^{-1}$ pc ($H_0 = 100h$ km sec $^{-1}$ Mpc $^{-1}$), being a fit to the unadorned unbinned data points; Fig. 2 shows the corresponding confidence regions (the green curves).

I have undertaken a similar analysis of the Caltech-Jodrell Bank 5 GHz survey, giving similar results, which survey cannot however be used in this context because it is not an all-sky one (Taylor et al. 1996; Jackson 2008).

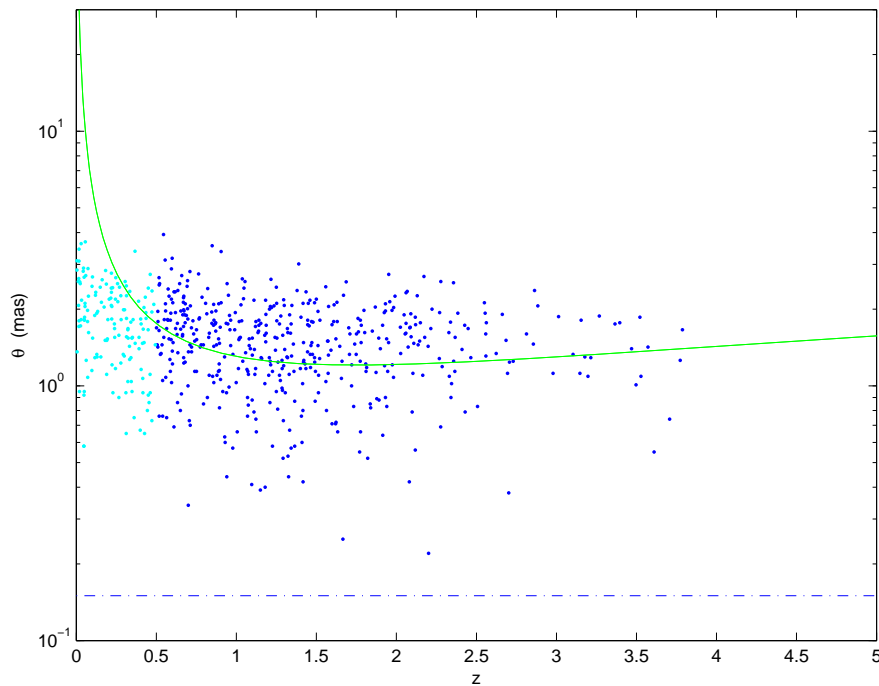


Figure 1. Angular-diameter/redshift diagram for the full sample of 468 sources (blue points), and the corresponding best-fitting curve $\Omega_m = 0.29$ and $d = 7.76h^{-1}$ pc. The blue dashdot line is an estimate of the resolution limit $\theta_{\text{lim}} = 0.15$ mas. The 145 cyan points have $z \leq 0.5$, and are not used in this investigation.

3. Anisotropy

To test isotropy, I have considered hemispheres, typically containing 234 ± 11 sources, which data points are allowed to determine Ω_m and d ; the values so determined now depend upon the particular hemisphere, defined by the Right ascension and declination (α, δ) of its axis. The coordinates used here are B1950, as listed in P85. Fig. 3 is a pseudocolor Mercator projection based upon an evaluation of Ω_m on a $5^\circ \times 5^\circ$ grid over the range $0^\circ \leq \alpha < 360^\circ$, $-60^\circ \leq \delta \leq 60^\circ$. The plot shows a pronounced asymmetry, a measure of which is the parameter $D = \Delta\Omega_m$ evaluated over opposing hemispheres. The global maximum value is $D_{\text{max}} = 0.626 - 0.135 = 0.491$ towards $(l, b) = (253.9, 24.1)^\circ$, which corresponds to the smaller value of Ω_m , indicated by the cyan ∇ mark in Fig. 3; the opposite direction is indicated by the grey ∇ mark.

The red and blue \times marks indicate the CMB dipole in the Local Group frame, with velocity 627 ± 22 km sec $^{-1}$, the ‘hot’ direction being $(l, b) = (276 \pm 3, 30 \pm 3)^\circ$ (Kogut et al. 1993). The proximity of these two directions is quite striking; however, the CMB dipole cannot be attributed to a peculiar velocity induced by gravitational attraction towards the region of enhanced density, which would be in the wrong direction, a point to which I shall return later. The features indicated by the Δ and square marks are for later reference. The figure reported by Antoniou & Perivolaropoulos

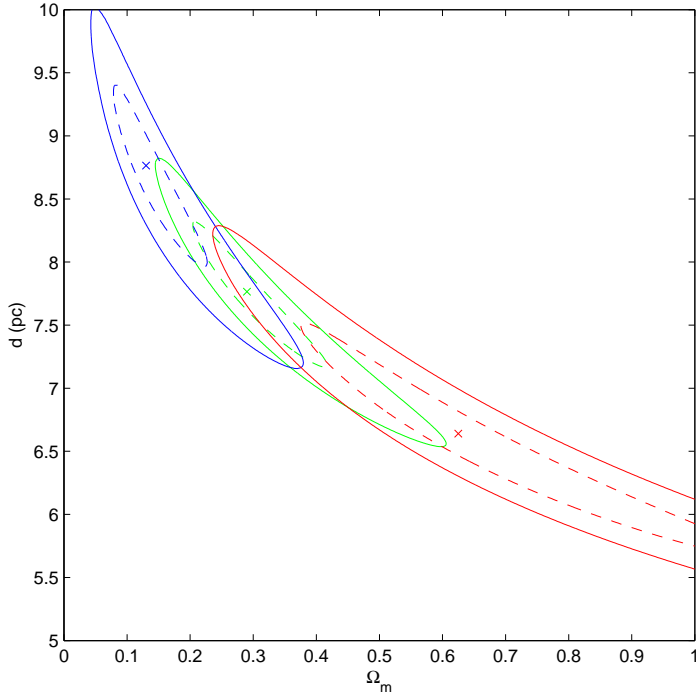


Figure 2. Confidence regions, one and two σ : green corresponds to the the full sample, blue and red to opposing extreme hemispheres. These are marginalized, so that projection on to each axis gives confidence intervals for the respective parameter.

(2010) is $D_{\max} = 0.30 - 0.19 = 0.11$ towards $(l, b) = (309_{-03}^{+23}, 18_{-11}^{+10})^\circ$, which again corresponds to the smaller value of Ω_m . The Union2 SNIa dataset covers the redshift range $0.015 \leq z \leq 1.4$ (Amanullah et al. 2010).

The blue and red confidence regions in Fig. 2 correspond to the hemispherical samples which determine $(\Omega_m)_{\min}$ and $(\Omega_m)_{\max}$, which samples I shall call S_{\min} and S_{\max} . I have considered one way in which the differences shown in Fig. 2 might be spurious. The fitting problem is close to degeneracy with respect to the parameters Ω_m and d , because we cannot use nearby sources, which would otherwise fix the latter (Jackson & Dodgson 1996). I have considered the possibility that there are in fact no significant differences between S_{\min} and S_{\max} , other than small accidental ones which due to the degeneracy are nevertheless large enough to bring about the divergences seen in Fig. 2. This possibility is discounted by the following considerations; I have further divided the two hemispherical samples, into $S_{\min}(z \leq 1.5)$ and $S_{\min}(z > 1.5)$, and similarly for S_{\max} . It is indeed the case that the low-redshift sub-samples are virtually identical, but in the high-redshift case there is a statistically significant difference: the two mean angular-sizes are $\bar{\theta}_{\min}(z > 1.5) = 1.35 \pm 0.05$ mas and $\bar{\theta}_{\max}(z > 1.5) = 1.56 \pm 0.06$ mas (1σ errors), which difference is not accounted for by a difference in the respective values of \bar{z} . The two values of $\bar{\theta}(z > 1.5)$ are the driving force behind the results presented here.

I have considered sensitivity to the exclusion of high-redshift sources, by looking at

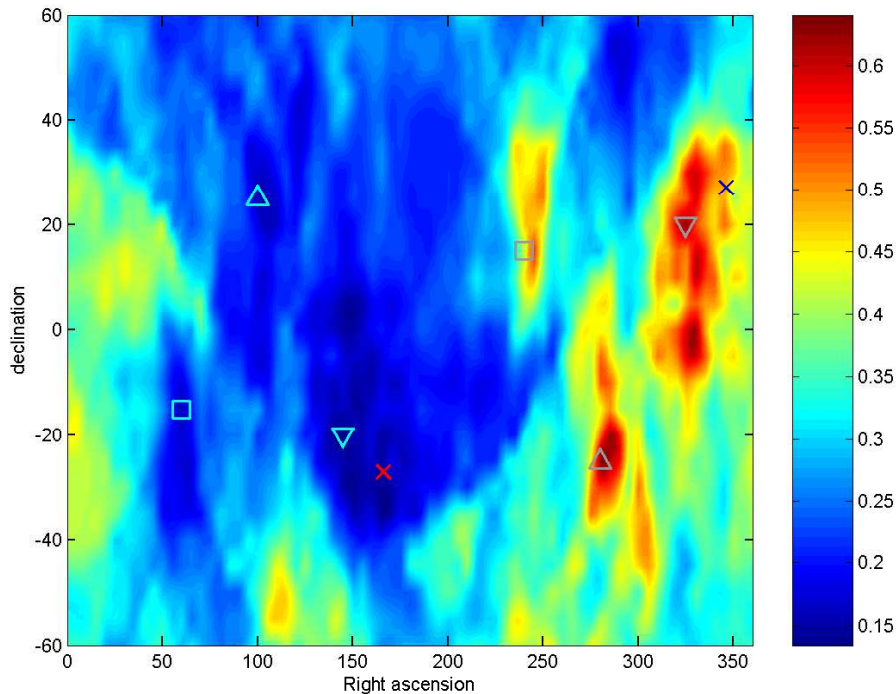


Figure 3. Pseudocolour plot showing the distribution of Ω_m over the sky; full sample of 468 sources, $0.5 < z \leq 3.787$. There are no prominent features in the polar regions. Crosses indicate the CMB dipole in the Local Group frame; the other symbols delineate prominent features for further reference.

restricted samples defined by $0.5 < z \leq z_{\max}$. The pattern remains reasonably stable as long as $z_{\max} \gtrsim 2.0$ (see Fig. 4); at $z_{\max} = 1.5$ there is little trace of the original structure. The results presented here thus do not depend upon a few high-redshift objects.

Could statistical fluctuations in the distribution of for example high-redshift sources between opposing hemispheres account for the apparent asymmetry? I have evaluated D_{\max} over an ensemble of mock samples, generated by randomizing source positions while leaving the corresponding redshift and angular-size data unchanged. The distribution of D_{\max} values so produced is broad, with a median value of 0.508. The above value $D_{\max} = 0.491$ is thus inconclusive. As an alternative test, I have first subjected the full list of 468 sources to a random shuffle, and then divided the list into two independent sub-samples, the first comprising all even-numbered members, the second all odd-numbered such members; Figs. 5 and 6 show the hemispherical distribution of Ω_m over the sky for the even and odd sub-samples respectively. If the prominent features delineated in Fig. 3 are due entirely to statistical fluctuations, then Figs. 5 and 6 would not be expected to show the same features, whereas it is quite clear that they do. Figures 5 and 6 are very similar; they are highly correlated, with a correlation coefficient of 0.413. Remembering that the even and odd sub-samples have no members in common, the probability of this situation arising by chance is less than 1×10^{-9} (see for example Freund & Walpole 1980). I conclude that the observed

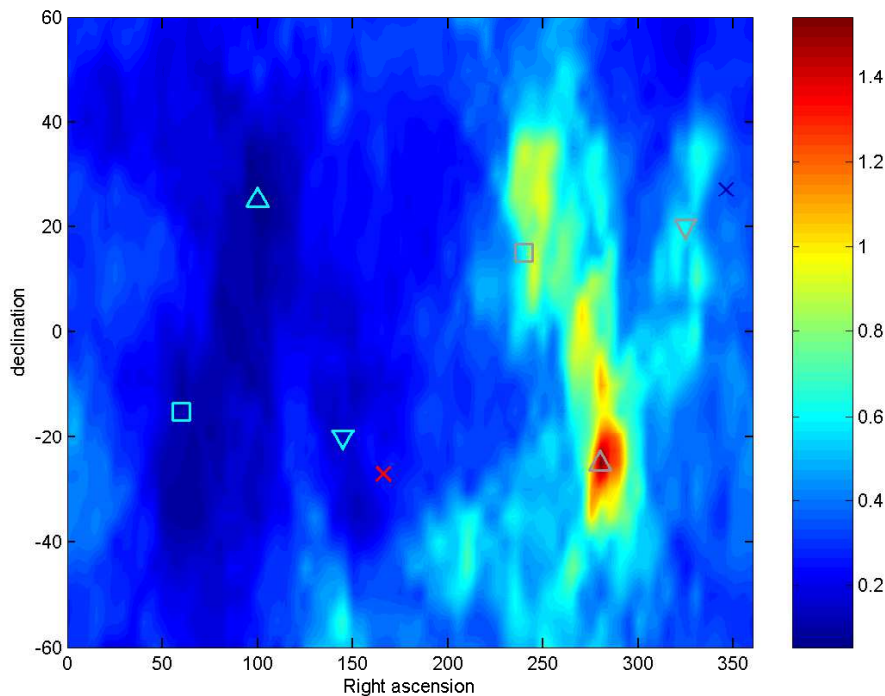


Figure 4. Pseudocolour plot showing the distribution of Ω_m over the sky; restricted sub-sample of 380 sources, $0.5 < z \leq 2.0$. The features highlighted in Fig. 3 have not been eliminated by dropping the high-redshift sources.

asymmetry is intrinsic. There are $468!$ distinct permutations of the original list, and I have examined a modest number of these; Figs. 5 and 6 represent a typical example.

The remaining possibility is that the apparent anisotropy is an instrumental effect, affecting all of the above-mentioned samples and sub-samples in like fashion. In this respect a suspect feature of the full sample of 468 sources is that not all of the flux measures derive from the same system; 339 are pure P85, in that they have both correlated and integrated flux densities listed in P85; the remaining 129 have correlated fluxes in P85, without the corresponding integrated fluxes; in these cases the latter were taken from the Parkes catalogue PKSCAT90 (Wright & Otrupcek 1990). As the correlated fluxes are the critical ones, I do not regard this as a serious deficiency; to confirm this I have discarded the ‘mixed’ sources and repeated the primary computation described above: Fig. 7 shows the Ω_m distribution determined by the set of pure P85 sources, which is very similar to Fig. 3. The anisotropy is clearly not an artefact of instrumental inhomogeneity. Finally there is the matter of uniformity of sky cover. Without the additional Parkes sources the pure P85 sample is deficient in southern-hemisphere ones ($\delta > -41.9^\circ$); with the additional Parkes sources the sample is uniform, the mean number per hemisphere being 233.95 ± 11.16 , very close to the binomial figure 234 ± 10.82 .

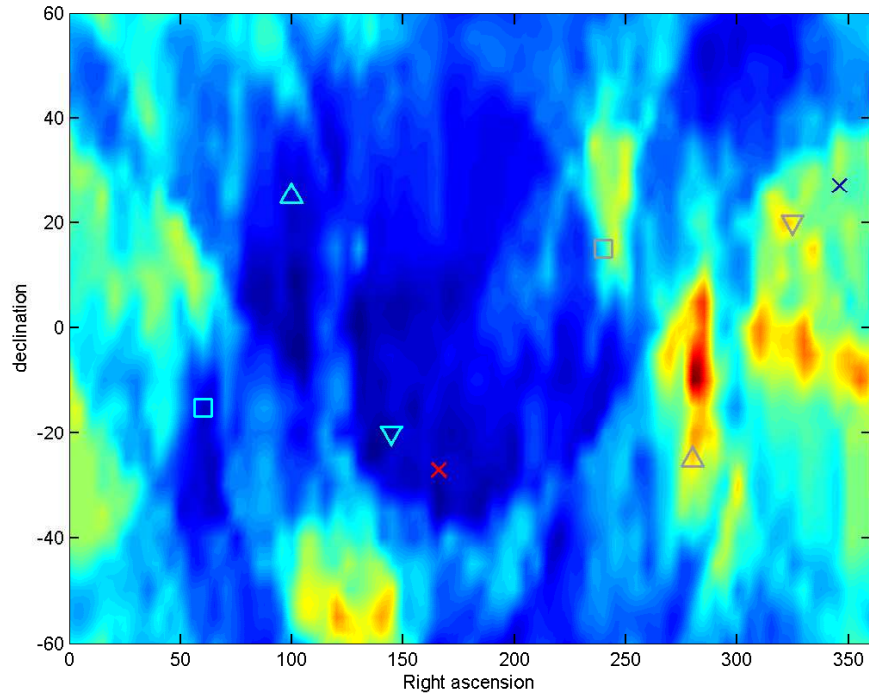


Figure 5. Pseudocolour plot showing the distribution of Ω_m over the sky; even sub-sample of 234 sources, see text.

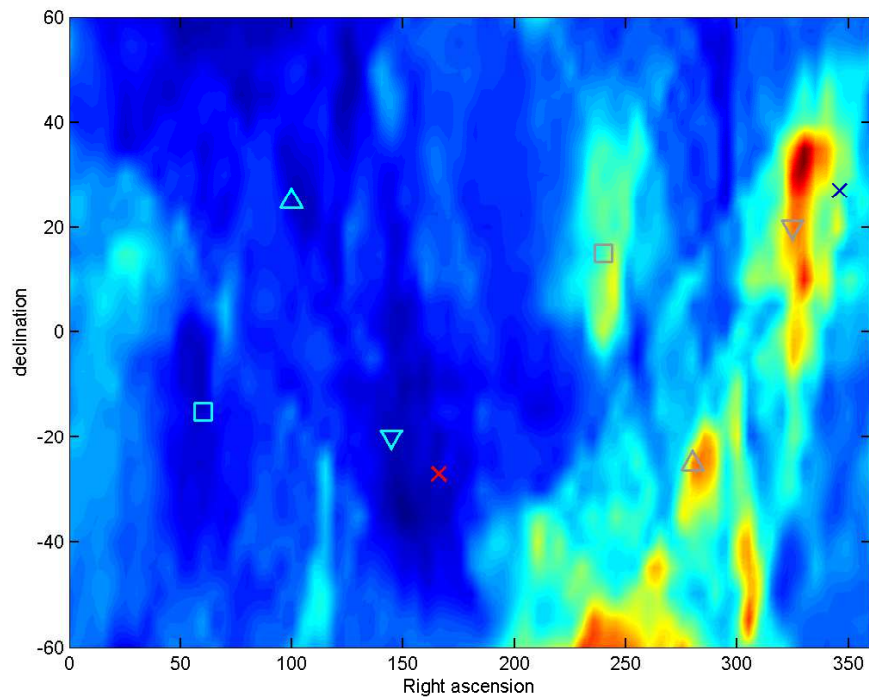


Figure 6. Pseudocolour plot showing the distribution of Ω_m over the sky; odd sub-sample of 234 sources, see text.

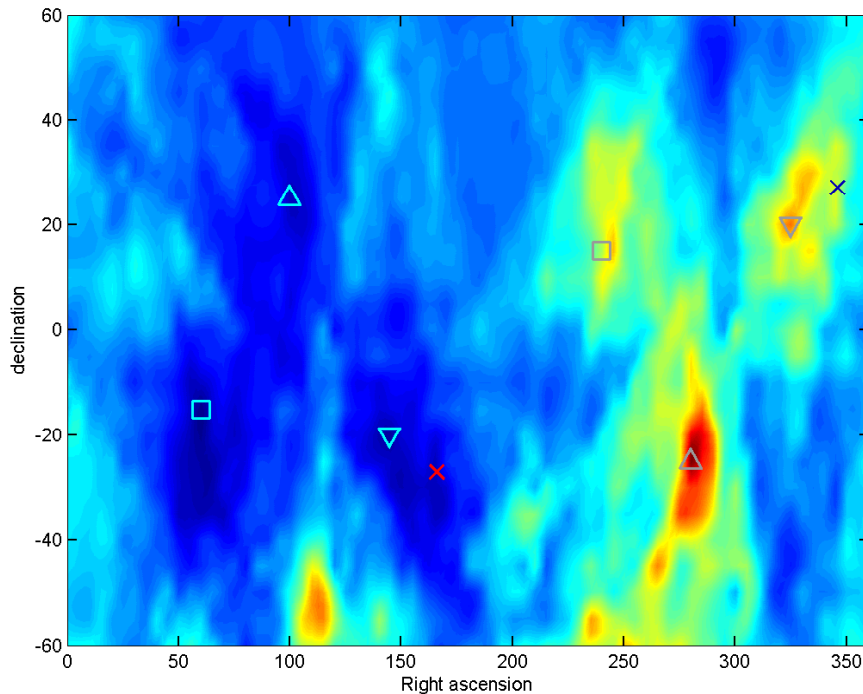


Figure 7. Pseudocolour plot showing the distribution of Ω_m over the sky; restricted sample comprising 339 pure P85 sources, $0.5 < z \leq 3.787$.

4. Interpretation and a toy model

We cannot of course maintain that the Universe is well-represented by a flat homogeneous isotropic Λ CDM model, but that a different such model is required according to direction. Nevertheless, I believe that these results mean that there is more dark matter in some directions than in others, whatever the geometrical setting. To see this, we consider a source represented by a small plane circular disc, perpendicular to the light-ray going from its centre to the observer. In vacuum, the bundle of rays going from the edge of the disc to the observer defines a cone with the observer at its apex; in the non-vacuum case the cone is refocussed by the gravitational attraction of the matter within it, as we trace the rays back towards the source, which refocussing has a magnifying effect. Indeed if the source is sufficiently distant then the cone begins to reconverge, and the apparent size of the source begins to increase (see for example Ellis & Tivon 1985). A reasonable explanation of the fact that the sources in the hemispherical sample S_{\max} appear to be systematically larger than those in S_{\min} , is that the rays in the direction of the former are passing through denser matter than those in the direction of the latter. In one or two simple cases an exact analytical treatment is possible (Jackson & Dodgson 1996), based upon the Ehlers-Sachs equation (Ehlers & Sachs 1959, Sachs 1961, Pirani 1965), which rederives some of the elementary cosmological results relating to distance.

The matter concentration revealed here cannot be behaving like a simple attractor,

because the motion of the Local Group would be towards the latter, whereas it appears to be in the opposite direction. However, this is exactly what an off-centre fundamental observer (at rest relative to the local Hubble flow) would expect to see in a spherically-symmetric dust-filled inhomogeneous model with a central concentration (Raine & Thomas 1981; Maartens et al. 1996a; Maartens et al. 1996b; Humpreys, Maartens & Matravars 1997). According to this picture the apparent motion of the Local Group is due largely to a peculiar cosmological redshift, rather than a peculiar flow (Paczynski & Piran 1990).

Large-scale coherent peculiar motions would be a feature of such a model, which must be compared with observations. The local such flow is believed to be due to the Great Attractor, a massive concentration of elliptical galaxies apparently at rest in the CMB frame, at a distance of $43.5h^{-1}$ Mpc towards $(l, b) = (307, 9)^\circ$ (Lynden-Bell et al. 1988); this result was based upon a sample of 400 elliptical galaxies closer than $80h^{-1}$ Mpc. Infall (rather than uniform bulk flow) gives a good account of the near-side flow; however, evidence for infall from the far side of the attractor is inconclusive (Dressler & Faber 1990). Watkins, Feldman & Hudson (2009) and Feldman, Watkins & Hudson (2010) examined a compilation of similar samples, and concluded that the mean peculiar motion of galaxies within a spherical volume of radius $c. 100h^{-1}$ Mpc is 416 ± 78 km s^{-1} , towards $(l, b) = (282 \pm 11, 6 \pm 6)^\circ$, and that this velocity appears to be increasing with distance. As the authors remark, a flow of this amplitude on such a large scale is not expected in the WMAP5-normalized Λ CDM cosmology.

Kashlinsky et al. (2008, 2009, 2010) have looked for CMB temperature fluctuations induced by the kinematic Sunyaev-Zel'dovich effect, from which the velocities of the associated clusters can be deduced. These authors report a positive detection with bulk velocities in the range 600 to 1000 km sec^{-1} towards $(l, b) = (283 \pm 14, 11 \pm 14)^\circ$, with most of the signal arising from a shell between $150h^{-1}$ and $600h^{-1}$ Mpc; such flows are not easily accomodated within the standard inflationary Λ CDM model (Atrio-Barandela et al. 2010). However, the latter results have been discounted by others (Keisler 2009; Osborne et al. 2011; Mody & Hajian 2012; Hand et al. 2012).

For purposes of comparison, I have considered a simple spherically symmetric zero-energy Newtonian model:

$$v^2 = \frac{2GM}{r(M)} + \frac{1}{3}\Lambda r(M)^2, \tag{3}$$

where $r(M)$ is the comoving radius of a sphere of mass M centred on the point of maximum concentration, and $v(r)$ is the radial velocity relative to the centre. Introducing $\bar{\rho}$ as the mean density within a sphere of radius r , equation (3) becomes

$$v^2 = \frac{8\pi G\bar{\rho}r^2}{3} + \frac{1}{3}\Lambda r^2. \tag{4}$$

We consider a snapshot and radial power series expansion about a point at r_0 :

$$v = v_0 + (r - r_0) \left(\frac{dv}{dr} \right)_0 + \frac{1}{2}(r - r_0)^2 \left(\frac{d^2v}{dr^2} \right)_0 + \dots \tag{5}$$

The first-derivative in equation (5) gives the local Hubble flow:

$$v_H = H_0 \Delta r = [-4\pi G A^{-1/2}(\bar{\rho} - \rho) + A^{1/2}]_0 \Delta r, \quad (6)$$

where $\Delta r = r - r_0$ and $A = 8\pi G \bar{\rho}/3 + \Lambda/3$. The second derivative gives a local radial peculiar flow; on a shell of radius Δr , this is (dropping the subscript):

$$v_B = \left\{ -\frac{A^{-1}}{r} [4\pi G(\bar{\rho} - \rho)]^2 + A^{-1/2} 4\pi G \left[\frac{2}{r}(\bar{\rho} - \rho) + \frac{d\rho}{dr} \right] \right\} \frac{\Delta r^2}{2}. \quad (7)$$

A positive value for v_B corresponds to peculiar motion away from the centre. We are considering distributions in which $\bar{\rho} - \rho > 0$ and $d\rho/dr < 0$, so that either sign is possible; for example, if $\bar{\rho} - \rho \gg |d\rho/dr|$ and $\bar{\rho}$ and ρ are not too different, the dominant term is

$$v_B \sim A^{-1/2} 4\pi G \rho \left(\frac{\bar{\rho} - \rho}{\rho} \right) \frac{\Delta r^2}{r} \sim \frac{1}{2} \left(\frac{\bar{\rho} - \rho}{\rho} \right) \frac{\Delta r}{r} H_0 \Delta r. \quad (8)$$

Taking $(\bar{\rho} - \rho)/\rho$ and $\Delta r/r$ to be 0.20, $\Delta r = 100$ Mpc and $H_0 = 70$ km sec⁻¹ Mpc⁻¹, equation (8) gives $v_B = 140$ km sec⁻¹. The main point of this rough estimate is to show that the model is not obviously at variance with the developing observational evidence, and that equations (6) and (7) are sufficiently flexible to accommodate possible contingencies.

5. Acknowledgments

It is a pleasure to thank Dr. William Stoeger of the Vatican Observatory Research Group, Steward Observatory, University of Arizona, who encouraged me to undertake this extension of the earlier work of myself and my colleagues; also to thank Richard Jackson for computational assistance.

6. References

- Amanullah R. et al., 2010, ApJ, 716, 712
 Antoniou I, Perivolaropoulos L, 2010, JCAP, 12, 012
 Atrio-Barandela F., Kashlinsky A., Ebeling H., Kocevski D., 2010,
 Journal of Physics: Conference Series, 229, 012003
 Clarkson, C. A., Maartens, R., 2010, Class. Quantum Grav., 27, 124008
 Dressler A., Faber S. M., 1990, ApJ, 354, 13
 Ehlers J., Sachs R., 1959, Z. Phys., 155, 498
 Ellis G. F. R., 2011, Class. Quantum Grav., 28, 164001
 Ellis G. F. R., Tivon G., 1985, Observatory, 105, 189
 Feldman H. A., Watkins R., Hudson M. J., 2010, MNRAS, 407, 2328
 Freund J. E., Walpole R. E., 1980, Mathematical Statistics. Prentice-Hall, New Jersey,
 p.444

- Gurvits L. I., 1994, *ApJ*, 425, 442
- Hand N., et al., 2012, preprint(arXiv:1203.4219)
- Humphreys N. P., Maartens R., Matravers D. R., 1997, *ApJ*, 477, 47
- Jackson J. C., 2008, *MNRAS*, 390, L1
- Jackson J. C., Dodgson. M., 1996, *MNRAS*, 278, 603
- Jackson J. C., Dodgson. M., 1997, *MNRAS*, 285, 806
- Jackson J. C., 2004, *JCAP*, 11, 007
- Jackson J. C., Jannetta A.L., 2006, *JCAP*, 11, 002
- Kashlinsky A., Atrio-Barandela F., Kocevski D., Ebeling H., 2008, *ApJ*, 686, L49
- Kashlinsky A., Atrio-Barandela F., Kocevski D., Ebeling H., 2009, *ApJ*, 691, 1479
- Kashlinsky A., Atrio-Barandela F., Ebeling H., Edge A., Kocevski D., 2010, *ApJ*, 712, L81
- Keisler R., 2009, *ApJ*, 707, L42
- Kogut A., et al., 1993, *ApJ*, 419, 1
- Kovalev Y. Y., et al., 2005, *AJ*, 130, 2473
- Longo M. J., 2012, preprint(arXiv:1202.4433)
- Lynden-Bell D., Faber S. M., Burstein D., Davies R. L., Dressler A., Terlevich R. J., Wegner G., 1988, *ApJ*, 326, 19
- Maartens R., Humphreys N. P., Matravers D. R., Stoeger, W. R., 1996, *Class. Quantum Grav.*, 13, 253
- Maartens R., Humphreys N. P., Matravers D. R., Stoeger, W. R., 1996, *Class. Quantum Grav.*, 13, 1689
- Marscher A. P., Shaffer D. B., 1980, *AJ*, 85, 668
- Mather, J. C., Fixsen, D. J., Shafer, R. A., Mosier, C., Wilkinson, D. T., 1999, *ApJ*, 512, 511
- Mody K., Hajian A., 2012, preprint(arXiv:1202.1339)
- Osborne S. J., Mak D. S. Y., Church S. E., Pierpaoli E., 2011, *ApJ*, 737, 98
- Paczynski B., Piran T., *ApJ*, 1990, 364, 341
- Pashchenko I. N., Vitrihshchak V. M., 2011, *Azh*, 2011, 88, 323
- Pearson T. J., Readhead A. C. S., 1981, *ApJ*, 248, 61
- Penzias A. A., Wilson R.W., 1965, *ApJ*, 142, 419
- Percival W. J. et al., 2002, *MNRAS*, 337, 1068
- Pirani F. A. E., 1965, in *Brandeis Lectures 1964 Vol. 1, General Relativity*. Prentice-Hall, New Jersey, pp. 331-362
- Preston R. A., Morabito D. D., Williams J. G., Faulkner J., Jauncey D. L., Nicolson G. D., 1985, *AJ*, 90, 1599
- Raine D. J., Thomas E. G., 1981, *MNRAS*, 195, 649
- Sachs R., 1961, *Proc. R. Soc. Lond.*, A264, 309
- Taylor G. B., Vermeulen R. C., Readhead A. C. S., Pearson T. J., Henstock D. R., Wilkinson P. N., 1996, *ApJS*, 107, 37
- Thompson A. R., Moran J.M., Swenson G.W., Jr, 1986, *Interferometry and Synthesis in Radio Astronomy*, Wiley, New York, p.13

Watkins R., Feldman H. A., Hudson M. J., 2009, MNRAS, 392, 743

Wilson R. W., Penzias A.A., 1967, Sci, 156, 1100

Wright A., Otrupcek R., 1990, PKSCAT90, 1990 Parkes Catalogue Australia Telescope National Facility, <http://www.parkes.atnf.csiro.au/research/surveys/pkscat90.html>